

## ARTICLE

# Identifying the Catalyst Chemical State and Adsorbed Species during Methanol Conversion on Copper Using Ambient Pressure X-ray Spectroscopies†

Received 00th January 20xx,  
Accepted 00th January 20xx

DOI: 10.1039/x0xx00000x

Baran Eren,<sup>\*a</sup> Christopher G. Sole,<sup>b</sup> Jesus S. Lacasa,<sup>a</sup> David Grinter,<sup>c</sup> Federica Venturini,<sup>c</sup> Georg Held,<sup>c</sup> C. Santiago Esconjauregui,<sup>d</sup> and Robert S. Weatherup,<sup>\*bce</sup>

Methanol is a promising chemical for the safe and efficient storage of hydrogen, where methanol conversion reactions can generate a hydrogen-containing gas mixture. Understanding the chemical state of the catalyst over which these reactions occur and the interplay with the adsorbed species present is key to the design of improved catalysts and process conditions. Here we study polycrystalline Cu foils using ambient pressure X-ray spectroscopies to reveal the Cu oxidation state and identify the adsorbed species during partial oxidation ( $\text{CH}_3\text{OH} + \text{O}_2$ ), steam reforming ( $\text{CH}_3\text{OH} + \text{H}_2\text{O}$ ), and autothermal reforming ( $\text{CH}_3\text{OH} + \text{O}_2 + \text{H}_2\text{O}$ ) of methanol at 200 °C surface temperature and in the mbar pressure range. We find that the Cu surface remains highly metallic throughout partial oxidation and steam reforming reactions, even for oxygen-rich conditions. However, for autothermal reforming the Cu surface shows significant oxidation towards  $\text{Cu}_2\text{O}$ . We rationalise this behaviour on the basis of the shift in equilibrium of the  $\text{CH}_3\text{OH}^* + \text{O}^* \rightleftharpoons \text{CH}_3\text{O}^* + \text{OH}^*$  caused by the addition of  $\text{H}_2\text{O}$ .

## 1. Introduction

The 'methanol economy' is envisaged as a sustainable future energy solution, an alternative to the currently prevalent 'oil economy', in which liquid methanol serves as a readily transportable energy vector to enable the transition away from fossil fuels.<sup>1</sup> Methanol conversion reactions, combined with methanol synthesis either from the exhaust products or other carbon containing waste-streams, promises an energy cycle that yields zero net emissions as long as the required energy input comes from renewable sources. Methanol's high H/C ratio make it particularly promising for on-board and swift  $\text{H}_2$  generation for supplying fuel cells in a much safer and space-efficient manner than the use of  $\text{H}_2$  storage tanks. Three conversion reactions are key to  $\text{H}_2$  generation from methanol: partial oxidation ( $\text{CH}_3\text{OH} + 0.5\text{O}_2 \rightarrow \text{CO}_2 + 2\text{H}_2$ ,  $\Delta H(298 \text{ °K}) = -192.2 \text{ kJ/mol}$ ), steam reforming ( $\text{CH}_3\text{OH} + \text{H}_2\text{O} \rightarrow \text{CO}_2 + 3\text{H}_2$ ,  $\Delta H(298 \text{ °K}) = 50 \text{ kJ/mol}$ ), and autothermal reforming (combination of steam reforming alongside total oxidation;  $\text{CH}_3\text{OH} + 1.5\text{O}_2 \rightarrow \text{CO}_2 + 2\text{H}_2\text{O}$ ,  $\Delta H(298 \text{ °K}) = -675.4 \text{ kJ/mol}$ ), which can be performed over Cu-based catalysts (reaction

formulas presented in simplified forms).<sup>2,3</sup> Amongst these, steam reforming is endothermic, requiring either external heating (above 180 °C) or autotherming via full oxidation to render it self-sustaining. For all of these processes, when performed at elevated temperatures to obtain high rates, forward and reverse water-gas shift ( $\text{CO} + \text{H}_2\text{O} \leftrightarrow \text{CO}_2 + \text{H}_2$ ,  $\Delta H(298 \text{ °K}) = -41 \text{ kJ/mol}$ ) can occur as side reactions and/or part of the overall reactions.<sup>2,3</sup> Understanding the chemical state of the catalyst over which these reactions occur, how this evolves during reaction, and the interplay with the adsorbed species present is key to rational catalyst design and process optimisation.

Surface-sensitive spectroscopies have been used to investigate the surface chemistry of the Cu catalyst both in ultra-high vacuum (UHV) and in the presence of gases, however almost all of these studies focus on methanol adsorption and methanol oxidation.<sup>4-11</sup> The effects of water (either as a reactant, impurity in methanol, or as a by-product) are often not discussed. Concerning methanol adsorption and methanol oxidation, early work on Cu surfaces in UHV includes structural studies using X-ray absorption spectroscopy (XAS), scanning tunnelling microscopy (STM), and infrared reflection absorption spectroscopy (IRRAS),<sup>4</sup> as well as adsorbate identification with X-ray photoelectron spectroscopy (XPS) and other techniques.<sup>5</sup> XAS, XPS, and sum-frequency generation (SFG) were also used under ambient methanol pressures and reaction conditions.<sup>6-11</sup> Both in UHV and in the presence of methanol vapour, methoxy ( $\text{OCH}_3$ ) is found to be the main reaction intermediate irrespective of whether single crystals, foils, powder catalysts, or supported nanoparticles are used.<sup>2</sup> It covers Cu surfaces at ambient pressures of methanol at room temperature (RT).<sup>9-10</sup> The other major adsorbed intermediate on the Cu surfaces is formate ( $\text{HCOO}$ ), which is typically observed under oxidising conditions.<sup>2</sup> Significant amounts of formaldehyde,

<sup>a</sup> Department of Chemical and Biological Physics, Weizmann Institute of Science, 234 Herzl Street, 76100 Rehovot, Israel.

Email: [baran.eren@weizmann.ac.il](mailto:baran.eren@weizmann.ac.il)

<sup>b</sup> Department of Chemistry, University of Manchester, Oxford Road, Manchester, M13 9PL, United Kingdom.

<sup>c</sup> Diamond Light Source, Didcot, Oxfordshire, OX11 0DE, United Kingdom.

<sup>d</sup> Department of Mechanical Engineering, Kingston University London, Friars Avenue, London SW15 3DW, United Kingdom.

<sup>e</sup> Department of Materials, University of Oxford, Parks Road, Oxford, Oxfordshire, OX1 3PH, United Kingdom.

Email: [robert.weatherup@materials.ox.ac.uk](mailto:robert.weatherup@materials.ox.ac.uk)

†Electronic Supplementary Information (ESI) available: [Additional AP-XPS and AP-NEXAFS spectra, gas dosing scheme]. See DOI: 10.1039/x0xx00000x

CO<sub>2</sub>, and molecular water have also been recorded as reaction products in the gas phase, under methanol oxidation conditions.

For a more complete understanding of the underlying processes occurring in methanol conversion, the role of water must also be carefully considered (as water will be present one way or another either as a reactant, product, or impurity in methanol). Therefore, the main goal of the present work is to identify the chemical state of Cu and the adsorbed surface species, including reaction intermediates, during the exposure of polycrystalline Cu foils to mixtures of methanol vapour, oxygen, and water vapour in the mbar pressure range using ambient pressure x-ray photoelectron spectroscopy (AP-XPS) and near edge x-ray absorption fine structure (AP-NEXAFS) spectroscopy. A recent catalysis study on the partial oxidation of methanol is a poignant illustration of the importance of the catalyst chemical state: the authors claim metallic Cu has a high selectivity towards CO<sub>2</sub>+H<sub>2</sub> formation,<sup>12</sup> which are the desired reaction products. Cu<sub>2</sub>O, on the other hand, results in the undesired combustion of methanol into CO<sub>2</sub>+H<sub>2</sub>O,<sup>12</sup> rather than the efficient generation of hydrogen gas.

In this study, we perform ambient pressure spectroscopic studies at a sample temperature of 200 °C and reactant pressures of a few tenths of mbar. We reveal that in the presence of methanol vapour and oxygen, even at oxygen-rich (1:1) partial pressure ratio conditions, the surface remains highly metallic. However, once water vapour is added into the gas admixture, the surface begins to oxidise towards Cu<sub>2</sub>O, which we attribute to a shift in the CH<sub>3</sub>OH(ad)+O(ad) ↔ OCH<sub>3</sub>(ad)+OH(ad) equilibrium on the surface towards the left hand side, as OH(ad) is readily available on the surface due to presence of water vapour. As a result, the ongoing removal of atomic oxygen from the surface by reaction with methanol is suppressed and this instead feeds oxidation of the Cu surface when all three gases are present. We also detect reaction intermediates such as methoxy, formate, hydroxyl, atomic oxygen, and lattice oxygen with AP-XPS under these reaction conditions. During our studies, when gases are present the surface becomes partly covered by adventitious hydrocarbons, and possibly oxygenated hydrocarbons, which makes the adsorbate coverage hard to assess. This contamination issue remains as a major challenge while working with wet gases in the ambient pressure surface science field.<sup>13</sup>

## 2. Experimental

AP-XPS and AP-NEXAFS measurements were performed at beamline B07-C of the Diamond Light Source (DLS), United Kingdom. The setup consists of three chambers separated by gate valves dedicated to sample introduction, sample preparation, and measurement. The measurement chamber includes a differentially-pumped ambient pressure hemispherical electron analyser (SPECS Phoibos 150 NAP) and a differentially pumped beamline interface that provides X-rays of 250–2800 eV, enabling measurements in the presence of methanol vapour, water vapour, and oxygen mixtures at pressures of up to ~10 mbar. The beamline exit slits were opened to 800 µm in the non-dispersive direction, and either 20 µm or 50 µm in the dispersive direction for XPS and NEXAFS measurements, respectively, which results in a spot size of approximately 100 µm x 100 µm. The combined energy resolution of the analyser and beamline is <0.4 eV for the energies used herein, as determined from the width of the

gaussian component of Voigt functions fitted to Au 4f spectra of gold films. Varying the exit slit size in the dispersive direction confirms that this is predominantly determined by the electron analyser for the photon energies used. Prior to experiments, both the preparation and measurement chambers had base pressures of around 8×10<sup>-10</sup> mbar, which increased to around 4–5×10<sup>-8</sup> mbar in the measurement chamber following the first dosing with the aforementioned vapours, due to residual vapour remaining in the background and sticking to the chamber walls. The high sticking coefficient of methanol and water to chamber walls is expected to lead to the displacement of hydrocarbons from the chamber walls, as seen be a gradual increase in hydrocarbon contamination on the samples, which was initially not present.

Cu foils (Alfa Aesar, 99.999% purity on metal basis) were cleaned with conventional Ar<sup>+</sup> sputtering (1.5 keV, 15 minutes) and annealing (300 °C to remove implanted Ar, 10 minutes) cycles in the preparation chamber prior to each set of experiments. The samples were transferred at 200–300 °C, and kept at 200 °C in all of the experiments (unless otherwise stated) as measured by a K-type thermocouple in contact with the foil. Methanol vapour, water vapour, and oxygen (in this order when multiple gases were dosed) were introduced into the measurement chamber through leak valves. Section S2 of the supporting information (SI) explains how all three gases were dosed and the approach taken to maintain the partial pressure ratios throughout hours of data acquisition. Dissolved air in liquid methanol and liquid water was removed by several thaw-freeze-pumping cycles.

For AP-XPS, photon energies ( $E_{ph}$ ) of 485, 730, and 1150 eV were used to produce photoelectrons with a kinetic energy ( $E_{kin}$ ) of approximately 200 eV in the C 1s, O 1s, and Cu 2p regions, respectively (inelastic mean free path,  $\lambda_{IMFP} \approx 6$  Å). All spectra were acquired with a pass energy of 20 eV. The binding energy scale for each spectra was referenced to simultaneously measured Cu 3p<sub>3/2</sub> core levels, setting the peak position to 74.9 eV. The presence of stray magnetic fields results in an uneven intensity profile across each XPS spectrum as low  $E_{kin}$  electrons are more affected by these. We eliminated this effect from our spectra during post processing of the data prior to fitting. In the rest of the paper, we only present C 1s and O 1s regions of the XPS spectrum as no CuO formation was detectable in the Cu 2p spectra (typically manifested as a 1.2 eV shift to higher binding energy with respect to Cu<sup>0</sup>), and Cu<sub>2</sub>O formation only leads to a modest shift in the Cu 2p peak position.<sup>14</sup>

NEXAFS spectra were acquired in Auger-Meitner electron yield (AEY) mode with a pass energy of 50 eV. The Cu L<sub>3</sub> edge between 930 and 950 eV is the region of interest in this study in order to distinguish between the Cu<sup>0</sup> and Cu<sub>2</sub>O oxidation states. The analyser was set to collect electrons with an  $E_{kin}$  of 600 eV to suppress contributions from the gas phase (as the gases used herein have Auger transitions with energies <530 eV)<sup>15</sup> and from low energy secondary electrons produced by inelastic scattering.  $\lambda_{IMFP} \approx 12$  Å for 600 eV electrons, however in contrast to XPS where the signal of interest arises from unscattered or elastically-scattered core electrons, the AEY mode Cu L<sub>3</sub> edge signal arises from inelastically-scattered primary Auger electrons. The probing depth is therefore expected to be intermediate between that of XPS, where inelastically scattered electrons are excluded, and total electron yield mode XAS, where inelastically scattered primary Auger electrons as well as low-

energy secondary electrons can contribute to the signal. We estimate the effective distance over which the energies of 920 eV Auger electrons are reduced to 600 eV in Cu as  $\sim 28 \text{ \AA}$ , using the continuously slowing down approximation and energy dependent stopping powers from Ashley et al.<sup>16</sup> Metallic Cu ( $\text{Cu}^0$ ) has a characteristic step-shape in the Cu  $L_3$  edge spectrum exhibiting multiple resonances, whereas  $\text{Cu}_2\text{O}$  has a dominant resonance at around 934 eV.<sup>17,18</sup> Gradual changes from metallic Cu to  $\text{Cu}_2\text{O}$  under reaction conditions can be monitored in our spectra and the  $\text{Cu}_2\text{O}$  amount roughly in the first 1-10 layers can be estimated from the linear combination of  $\text{Cu}^0$  and  $\text{Cu}_2\text{O}$  reference curves.

### 3. Results and discussion

#### 3.1 Methanol adsorption

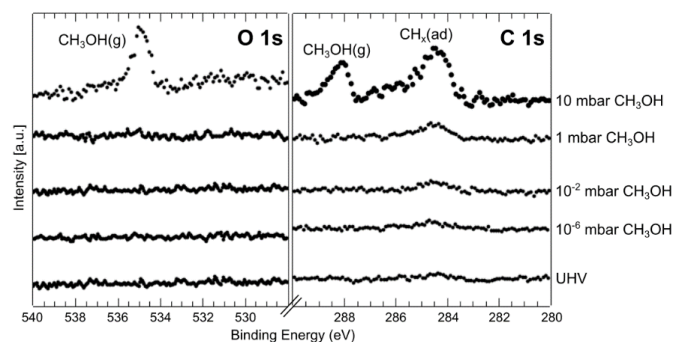


**Fig. 1** O 1s and C 1s regions of XPS spectra at 200 °C sample temperature in the presence of methanol vapour at various pressures. Coverages of methanol derivatives such as methoxy and formate are below the XPS detection limit under these conditions. The only discernible features are gas phase methanol visible at 10 mbar of methanol (at  $>535 \text{ eV}$  and  $>288 \text{ eV}$ ), and hydrocarbon contamination which is present across all conditions ( $\sim 284.4 \text{ eV}$ ).

We first performed methanol adsorption experiments to identify the peak positions of adsorbed methanol derivatives on the cleaned polycrystalline Cu surface. Fig. 1 shows the O 1s and C 1s core level regions which contain no discernible features at  $\text{CH}_3\text{OH}$  pressures of  $\leq 1 \text{ mbar}$  other than the gradual emergence of a hydrocarbon contamination ( $\text{CH}_x$ ) peak at  $284.4 \pm 0.1 \text{ eV}$ . We can thus conclude that the steady state methoxy and formate coverage on Cu at 200 °C is  $<1\%$  of a monolayer, as was previously confirmed at 400 °C.<sup>8</sup> Peaks related to gas phase methanol are only discernible at 10 mbar, at apparent binding energies above 535 eV and 288 eV, with the exact position dependant on the work function of the sample.<sup>19</sup> The detection of gas phase methanol peaks at lower pressures in our previous studies<sup>10</sup> is attributable to the larger volume of the illuminated gas in front of the AP-XPS nozzle: We estimate the volume to be  $\sim 2$  orders of magnitude lower with the choice of the slits and the nozzle-sample distance (250  $\mu\text{m}$ ) we use in the current study compared to our previous work in Ref.<sup>10</sup>.

Fig. 2 shows the steady state adsorption of methanol at 65 °C. In terms of the adsorbed species, these spectra are similar to those published in Ref. 10, with the addition of some hydrocarbon contamination in the present case. In the C 1s region, methoxy and formate species appear at roughly  $285.2 \pm 0.2 \text{ eV}$  and  $288.1 \pm 0.2 \text{ eV}$ , respectively. In the O 1s region, the peak positions of the methoxy and formate species are very close to each other; therefore they

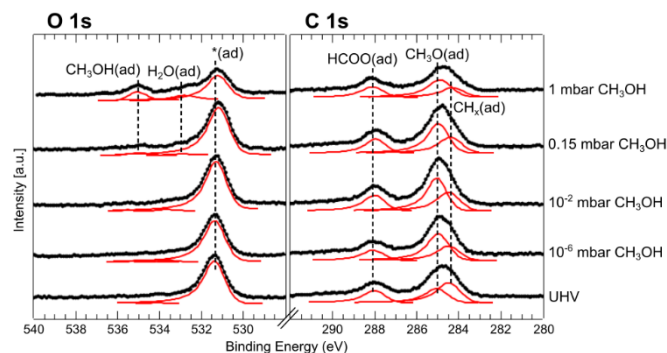


**Fig. 2** O 1s and C 1s regions of XPS spectra at 65 °C sample temperature in the presence of methanol vapour at various pressures. In the C 1s region, methoxy and formate appear at  $\sim 288.1 \text{ eV}$  and  $\sim 285.2 \text{ eV}$ , respectively. Note that oxygenated hydrocarbon contamination can appear in the same position as formate.<sup>13</sup> In the O 1s, the peak positions are very close to each other; therefore we fitted them as a single convoluted peak at  $531.3 \text{ eV}$ , marked with  $*(\text{ad})$ . Adsorbed OH, originating from cross contamination of water vapour, might also have some contribution to the intensity of this  $*(\text{ad})$  peak. At 1 mbar, there is an additional peak at  $535.1 \text{ eV}$ , which could potentially be molecular methanol, with the corresponding C 1s feature convoluted inside the peak at  $\sim 288.1 \text{ eV}$ . Adsorbed molecular water, a cross contaminant from previous experiments, appear at  $\sim 533.1 \text{ eV}$ . Black dots are the raw data, red curves are the fitted components, and black solid curves are the sum of the red curves.

have been fitted as a single convoluted peak at  $531.3 \pm 0.1 \text{ eV}$  (i.e., the analysis of their relative intensities is more reliable in the C 1s region).<sup>18</sup> We used slightly asymmetric lineshapes ( $\alpha=0.05$ ) for adsorbed species; a similar approach was taken in adsorption studies at cryogenic temperatures in Ref. 20. Such an asymmetric tail is attributable to vibrational losses,<sup>21</sup> rather than any asymmetry related to interaction with the d-electrons close to Fermi level, which Cu lacks. The Doniach-Šunjić-like line shapes of these peaks were constrained with boundaries in the rest of our analysis, whereas the peak positions were not strictly constrained to account for slight shifts that may arise from reconstruction of the Cu surface. In our previous work on Cu(100),<sup>10</sup> we measured methoxy at  $530.3 \text{ eV}$  and  $285.3 \text{ eV}$ , and formate at  $531.4 \text{ eV}$  and  $287.5 \text{ eV}$ . The slightly higher binding energy in the present study is attributable to variation in the surface coordination number: For instance, adsorption studies in UHV resulted in formate peak positions at  $531.3 \text{ eV}$  and  $287.3 \text{ eV}$  on Cu(111) whose coordination number is 9, compared to  $531.6 \text{ eV}$  and  $288.0 \text{ eV}$  on Cu(110) whose coordination number is 7.<sup>22</sup> In the same study, methoxy peaks were observed at  $530.9 \text{ eV}$  and  $285.5 \text{ eV}$  on Cu(110).<sup>22</sup> Our repeatedly sputtered and low-temperature annealed polycrystalline surfaces are expected to be rich in low-coordinated step and kink sites. The peak positions we observe in the C 1s region thus give some tentative indication that formate is forming on these low-coordinated and more active sites, whereas methoxy is forming mostly on flat terraces, with the methoxy peak appearing at a low binding energy ( $285.2 \text{ eV}$ ) consistent with adsorption on {111} terraces (the lowest energy surface orientation for Cu). We note that to unequivocally confirm the suggested adsorption behaviour requires techniques that are more sensitive to the coordination

number of adsorption sites such as infrared spectroscopy, however this is beyond the scope of the present study.

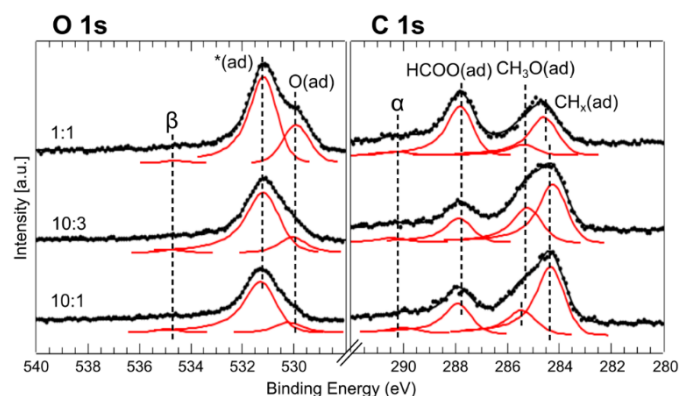


**Fig. 3** O 1s and C 1s regions of XPS spectra at 200 °C sample temperature in the presence of 0.15 mbar methanol vapour and 0.015 mbar, 0.045 mbar, or 0.15 mbar oxygen (presented as partial pressure ratios). As the oxygen partial pressure in the gas phase increases, the intensity of the peak at ~529.9 eV attributed to adsorbed atomic oxygen increases, and more formate (~287.8 eV) forms on the surface, whilst there is a corresponding reduction in the methoxy (~285.4 eV) peak. O 1s spectra were acquired approximately 1.5 hours after O<sub>2</sub> introduction into the chamber, which already contained the methanol vapour. C 1s spectra were acquired at a slightly different times after O<sub>2</sub> introduction: Bottom and top spectra were acquired within 45 min of O<sub>2</sub> introduction, whereas the middle spectrum was acquired after 2 hours. Peaks with the letters β and α may originate from gas phase formaldehyde, a product of this reaction. Black dots are the raw data, red curves are the fitted components, and black solid curves are the sum of the red curves.

At 1 mbar and 65 °C, an additional peak is observed at 535.1 eV (Fig. 2 top panel), which we assign to adsorbed molecular methanol, with its feature in the C 1s region assumed to be convoluted with the formate peak at around 288 eV. Although some contribution to this peak from methanol vapour cannot be excluded, we note that our measurements of methanol adsorption at 200 °C show no gas phase species at 1 mbar. Adsorbed molecular methanol at cryogenic temperatures has however previously been reported at binding energies of 533.8 eV and 287.4 eV.<sup>23</sup> The appearance at higher energies in our case, may be attributable to molecular methanol forming as an ad-layer on top of an underlying methoxy and formate mixture. The appearance of a weak peak at 533.1 eV under this condition, indicates that some molecular water also adsorbs onto the surface. The peak at 531.3 eV thus also likely has some contribution from adsorbed OH in addition to methoxy and formate. The presence of the formate peak in Fig. 2 (as also observed in Ref.<sup>10</sup>) is somewhat surprising given the absence of oxidising species in the gas phase. There are three potential origins of the required oxidising species: 1- X-ray beam dissociation of methanol. However this can be largely excluded given the relatively low X-ray intensity of our measurements and that a gradual increase in formate intensity is not observed. Moreover, changing the position on the sample does not cause any significant change in the spectra. A common feature of beam-induced chemistry is carbonate formation, with peak positions at 289.3 eV and 532 eV,<sup>24</sup> that are also not observed here. 2- Residual water dissolved in the methanol or that is displaced from the

chamber walls by methanol adsorption. However, this is not expected to contribute significantly as the water + methanol reaction is endothermic with an onset usually above 180 °C. 3- Oxygen dissolved in the Cu crystal. We do not observe any atomic oxygen peak after the sputtering and annealing treatment, but this does not rule out the possibility that subsurface oxygen diffuses to the surface under reaction conditions and reacts immediately with methanol to form formate.<sup>10</sup> We note that Cu has a high solubility for oxygen and the foil purity cited by suppliers is on metal basis. Moreover, each time the foil is used in the experiments, oxygen species present at the surface are dissolved into the bulk, increasing the oxygen content. The experimental history of the foil (e.g., the methanol oxidation experiments in Section 3.2 were performed prior to adsorption experiments at 65 °C) can thus influence the chemical species observed at the surface. There is an alternative explanation to this peak which does not require the presence of oxidising species: A recent study suggests that the accumulation of oxygenated hydrocarbons may yield XPS peaks similar to those of formate: During steady-state water vapour adsorption, the accumulation of significant amounts of adventitious oxygenated hydrocarbons on copper oxides was observed.<sup>13</sup> This is attributable to the displacement of oxygenated hydrocarbons from the chamber walls, rather than their formation under the experimental conditions used. In view of this, we cannot exclude a contribution of such adventitious oxygenated hydrocarbons to the peaks assigned to formate.

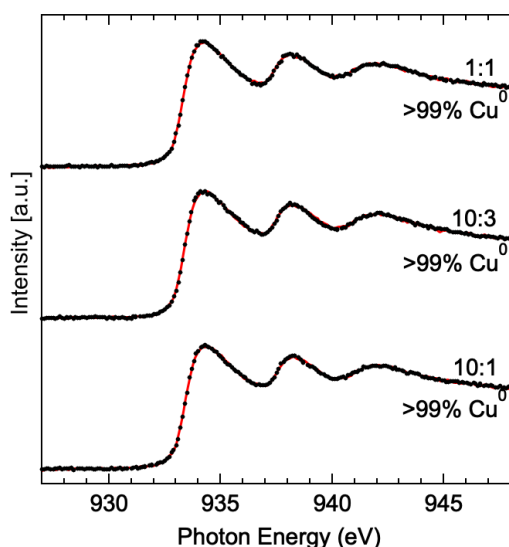
### 3.2 Methanol oxidation

Fig. 3 shows the O 1s and C 1s regions of the XPS spectra in the presence of 0.15 mbar methanol vapour with various partial pressures of oxygen (10:1, 10:3, and 1:1 methanol to oxygen ratio) at 200 °C sample temperature. The most significant new feature observed is the peak at 529.9 ± 0.1 eV. This lies between the lattice oxygen and chemisorbed atomic oxygen peaks that were previously assigned at 530.2 eV and 529.4 eV, respectively on the Cu(111) surface.<sup>18</sup> The 529.9 ± 0.1 eV peak is likely a convolution of both of these peaks due to a lower energy resolution in the present study (as it will be shown later, the main contribution to this peak comes from adsorbed atomic oxygen). The peak intensity increases with oxygen partial pressure, consistent with increasing adsorption of atomic oxygen and perhaps slightly more oxidation of the Cu surface. As expected, the formate intensity is significantly higher than the methoxy intensity at the highest oxygen partial pressure conditions. We note however that these measurements are not suitable for quantitative comparison as each spectrum was acquired after different oxygen exposure times, as indicated in the figure captions. Time-resolved spectra show an increase in adsorbed oxygen with time (Fig. S1-left in SI), hence the uncertainty for quantitative analysis, but nevertheless the general trends observed still hold.

The peaks at 285.4 eV and 287.8 eV observed in the C 1s region of Fig. 3, are attributable to methoxy and formate, respectively. This corresponds to a 0.2-0.3 eV shift for both species (positive for methoxy and negative for formate) compared to the peak positions in Fig. 2, such that they are both closer to the positions observed on Cu(110) which has intermediate coordination number. This indicates that both species are distributed across the surface during the methanol oxidation reaction, rather than the preferential formation



of formate on the low-coordinated sites and methoxy on more highly-coordinated sites, as suggested for Fig. 2.



**Fig. 4** Cu  $L_3$  edge of the x-ray absorption spectra at 200 °C sample temperature in the presence of 0.15 mbar methanol vapour and 0.015 mbar, 0.045 mbar, or 0.15 mbar oxygen (presented as partial pressure ratios). The three strong resonances are consistent with a strong metallic character, with linear combination fitting indicating <0.5%  $\text{Cu}_2\text{O}$  for all of the partial pressure ratios.

Low-intensity features are also detectable at around 290 eV and 534.7 eV (marked as  $\alpha$  and  $\beta$ ), which are consistent with gas phase formaldehyde ( $\text{CH}_2\text{O}$ , reaction co-product), which has also been observed in previous AP-XPS studies performed under such conditions.<sup>8,10,11</sup> However, as noted earlier, the setup used herein is rather insensitive to gas phase species at low pressures. Among the adsorbed species, such a high XPS binding energy in the C 1s region is only consistent with a carbonate-like species. It is not possible to discern carbonate-like species in the O 1s region as they will appear inside the higher binding energy tail of the broad peak at 531.3 eV. However, carbonate formation would only account for the 290 eV peak leaving the 534.7 eV peak unassigned. We exclude adsorbed CO and  $\text{CO}_2^{\delta-}$  species as these have previously been observed at a binding energy of 286.1 eV for CO on metallic Cu (with a satellite 2.2 eV above), 287.9 eV for CO on  $\text{Cu}_2\text{O}$  (with a satellite 2.1 eV above), and 289 eV for  $\text{CO}_2^{\delta-}$  either on Cu or  $\text{Cu}_2\text{O}$ .<sup>18</sup> Moreover, both CO and  $\text{CO}_2$  have low adsorption energies on Cu, making their appearance in an XPS spectrum at 200 °C as adsorbed species unlikely. In other words, CO and  $\text{CO}_2$  are very likely to form; but should immediately desorb to the gas phase. In short, these  $\alpha$  and  $\beta$  peaks can be best explained by gas phase  $\text{CH}_2\text{O}$  formation, which would correspond to a significant amount of formaldehyde formation. Indeed, similar gas mixtures were previously found to yield a significant amount of formaldehyde for sample temperatures of 200 °C and above.<sup>8,11</sup>

NEXAFS measurements at the Cu  $L_3$  edge were performed to estimate the level of oxidation (Fig. 4) in the presence of methanol and oxygen. These were fitted using linear combinations of reference spectra acquired for pure Cu and pure  $\text{Cu}_2\text{O}$ . For all partial pressures (10:1, 10:3, and 1:1 ratios of  $\text{CH}_3\text{OH}:\text{O}_2$ ) the chemical state is found to be >99% metallic. The surface still remains almost completely metallic even after extended exposures to the gas admixtures (Fig.

S1-right). Given that NEXAFS in AEY mode is less surface-sensitive than our XPS measurements ( $E_{\text{kin}} = 200$  eV), the first surface layer could have slightly more oxidic character, but this is still expected to be <3% of  $\text{Cu}_2\text{O}$ . We therefore conclude that the peak at 529.9 eV in Fig. 3 originates predominantly from adsorbed atomic oxygen, with only very minor contributions from lattice oxygen. We note that this atomic oxygen may be adsorbed not only on the topmost surface, but also at other interfaces such as grain boundaries.

The changes in the Cu chemical state can be better understood in the context of recent CO oxidation studies using AP-XPS and AP-NEXAFS.<sup>18</sup> In Ref. 18, the Cu surface becomes oxidised even at more oxygen-lean (i.e., lower  $\text{O}_2$  partial pressures) and lower temperature conditions than used herein. This indicates methanol vapour is a much more effective reducing agent than CO gas, either via methoxy formation, or methoxy further reacting with atomic oxygen to form formaldehyde, formate, and  $\text{CO}_2$ . CO oxidation is often considered a prototypical reaction for more complex oxidation reactions,<sup>25</sup> but the substantial difference in adsorption energy of CO and other molecules such as methoxy calls such an approach into question for Cu surfaces. Methoxy adsorbs on the surface via the O atom (metal- $\text{OCH}_3$ ), whereas CO adsorbs via the C atom (metal-CO). This different adsorption geometry makes a very substantial difference in adsorption energies: For instance, the methoxy binding energy on Cu(111) and on Cu(100) was calculated to be over 1 eV;<sup>26</sup> much higher than the CO adsorption energy of 0.5–0.6 eV.<sup>27</sup> This is manifested in the inability of CO to reduce  $\text{Cu}_2\text{O}$  or remove surface oxygen, i.e. the Sabatier principle, given the adsorption energy of atomic oxygen on Cu is 1.5–2.1 eV.<sup>28</sup> We find here that methanol is very effective in removing atomic oxygen from the surface and reducing  $\text{Cu}_2\text{O}$ , as also previously observed in liquid phase experiments.<sup>29</sup> Direct comparison of the current results with Ref. 18 provides a possible explanation for why Cu is a good catalyst for the methanol oxidation but suffers swift deactivation during CO oxidation. It has even been suggested that CuO may be able to form under CO oxidation conditions which poisons the surface.<sup>30</sup> We did not detect any CuO formation in the mbar pressure range,<sup>18</sup> but it is feasible that this results from the equilibrium shift as the bar pressure range is approached, as observed for Cu in the presence of pure  $\text{O}_2$ .<sup>31</sup> Such deactivation is not expected for methanol oxidation because of the efficiency of methanol in reducing Cu as shown in the present work.

Our oxidation state analysis in this section can be directly compared with other literature. Ref. 11 (total pressure = 0.1 mbar,  $\text{CH}_3\text{OH}/\text{O}_2 = 3/1$ ,  $T = 150$  °C and 250 °C) agrees that the surface is metallic based on X-ray-excited Cu LMM Auger spectra. However, they claim a substoichiometric oxide formation at 250 °C, with an O 1s peak at 531.2 eV, and no corresponding feature in the C 1s region, excluding the possibility of formate. If a substoichiometric oxide is present (on the surface or in the subsurface), it will have hybridised electronic states of  $\text{Cu}_2\text{O}$  and  $\text{Cu}^0$  nature, which can be monitored through the resonances in NEXAFS O K edge spectra.<sup>7,18</sup> Substoichiometric oxide formation would however be expected to be accompanied by some changes to the metallic resonances of the Cu  $L_3$  edge, however this is not seen in our measurements (Figure 4); therefore we exclude significant substoichiometric oxide formation for our conditions. It should also be noted that the original paper mentioning this substoichiometric oxide phase assigned its O 1s peak

to the same position as the  $\text{Cu}_2\text{O}$  peak, close to 530 eV.<sup>7</sup> Other key studies of methanol oxidation were performed at higher temperatures (400 °C rather than the 200 °C used herein), where  $\text{Cu}_2\text{O}$  is observed on the surface alongside a significant amount of water formation.<sup>7,8</sup> Higher temperatures decrease the  $\text{H}_2$  yield in favour of  $\text{H}_2\text{O}$ ,<sup>11</sup> which is expected to correlate with the extent of surface oxidation. Thus if surface oxidation proceeds with reaction time,<sup>12</sup> the selectivity towards  $\text{H}_2$  should correspondingly decrease. At 200 °C, however, the surface remains almost fully metallic even after hours of exposure to 5:1  $\text{CH}_3\text{OH}:\text{O}_2$  (Figure S1).

### 3.3 Inclusion of water

Steam reforming and autothermal reforming of methanol involves mixtures of methanol and water vapours in the gas admixture. We start our analysis with reference XPS spectra acquired in the presence of water vapour: Fig. S2 shows the O 1s and C 1s regions of the XPS spectra in the presence of water vapour dosed into the measurement chamber whose walls are already 'contaminated' with methanol from previous experiments. In contrast to the pure methanol adsorption experiments at 200 °C (Fig. 1), methanol derivatives are now seen to adsorb on the surface from residual methanol in the gas phase during water exposure. The peak at 531.2 eV appears slightly broader which is attributable to more OH species adsorbing on the surface. Another broad peak is observed at 533.1 eV, typical of adsorbed molecular water species, together with the gas phase  $\text{H}_2\text{O}$  peak at an apparent binding energy of >535 eV.

When co-dosing methanol and water vapour, we must return to the issue of hydrocarbon contamination once again. Methanol and water adsorption on the chamber walls displaces hydrocarbons which then accumulate on the surface. Unfortunately, this hydrocarbon contamination (often referred to as adventitious carbon) is a common problem in ambient pressure surface science as it is not fully removed with conventional chamber bake-outs (>110 °C, 48 hours). In our experience, the ignition of a nitrogen plasma prior to the conventional bake-out is effective in removing these hydrocarbons,<sup>32</sup> but this is not always possible in shared user facilities due to constraints of the experimental schedule. When both methanol and water vapour are present, the XPS spectra are therefore dominated by hydrocarbon contamination, blocking most of the adsorption sites (Fig. S3). The copper oxidation state is found not to change during these methanol and water co-dosing experiments remaining highly metallic (Fig. S4).

We finally turn to the XPS and NEXAFS acquired when all three gases are presents (Fig. 5 and 6) for studying autothermal reforming of methanol. Hydrocarbon contamination is less problematic in this case due to the presence of  $\text{O}_2$  in gas phase which helps to burn away some of the hydrocarbons (Fig. 5), avoiding their accumulation over time. To understand the effect of water addition into the methanol and oxygen gas admixture, Fig. 5 and 6 should be directly compared to Fig. 3 and 4. The most significant difference is seen in the copper oxidation state: As the oxygen partial pressure is increased,  $\text{Cu}_2\text{O}$  starts to form on the surface, as seen in the upper two plots of Fig. 6 by the emergence of the strong single resonance at ~934 eV which is characteristic of  $\text{Cu}_2\text{O}$ . Linear combination fitting of the Cu  $\text{L}_3$  edge NEXAFS spectra yields >50%  $\text{Cu}_2\text{O}$  for 5:5:1 and 1:1:1  $\text{CH}_3\text{OH}:\text{H}_2\text{O}:\text{O}_2$  partial pressure ratios, which could correspond to full coverage of

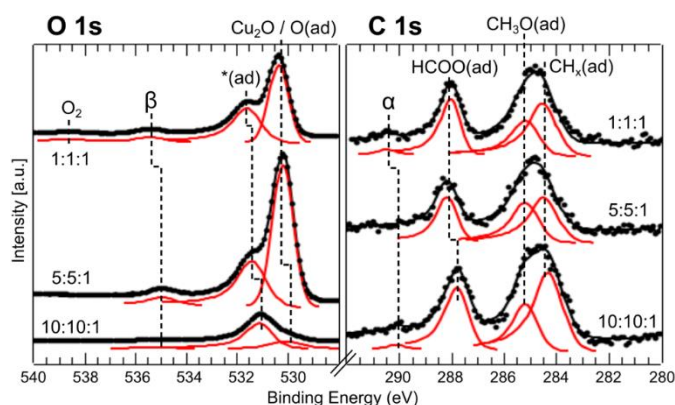


**Fig. 5** O 1s and C 1s regions of the XPS spectra at 200 °C sample temperature in the presence of 0.15 mbar methanol vapour, 0.15 mbar water vapour, and 0.015 mbar, 0.03 mbar, or 0.15 mbar oxygen (presented as partial pressure ratios  $\text{CH}_3\text{OH}:\text{H}_2\text{O}:\text{O}_2$ ). Compared to Fig. 3, the lowest energy peak in the O 1s region dominates the spectra at higher oxygen partial pressures despite the  $\text{CH}_3\text{OH}:\text{O}_2$  ratios being the same, with this difference attributable to the presence of water vapour. This peak also shifts to significantly higher binding energies (530.4 eV), suggesting that the adsorbed atomic oxygen becomes lattice oxygen of  $\text{Cu}_2\text{O}$ . Assuming  $\alpha$  and  $\beta$  peaks are gas phase formaldehyde, their shifts in apparent binding energy relate to the changes in the work function as the surface oxidises. It is also possible to observe slight shifts in the position of the  $\ast(\text{ad})$  peak (convoluted peak consisting of adsorbed methoxy, formate, and OH species) in the O 1s region and the formate peak in the C 1s region. The top and bottom O 1s spectra were acquired 1 hour after the introduction of all three gases, whereas the middle spectrum was acquired after 3.5 hours (due to a loss of X-ray beam). Similarly, the top and bottom C 1s spectra were acquired 0.5 hours after the introduction of the gases, whereas the middle spectrum was acquired after 3 hours. Longer waiting before the acquisition results in a more oxidised surface as discussed in Fig. S5. Black dots are the raw data, red curves are the fitted components, and black solid curves are the sum of the red curves.

the surface with  $\text{Cu}_2\text{O}$ , given AEY mode NEXAFS can include significant subsurface contributions. We note that substoichiometric oxide ( $\text{Cu}_x\text{O}$ ,  $x > 2$ ) may be present but is not uniquely identifiable from our linear combination fitting of the Cu  $\text{L}_3$  edge or the corresponding Cu 2p and O 1s XP core level spectra. This would require further analysis of the O K edge or valence band spectra<sup>7</sup> beyond the scope of the present work. Oxidation of the Cu surface gradually continues with longer exposures (Fig. S5), however  $\text{CuO}$  is still not detected in any of the spectra.

The influence of  $\text{Cu}_2\text{O}$  formation is also seen in the peak positions of the XPS spectra shown in Fig. 5. The most significant change is the peak at 529.9 eV shifting to 530.4 eV as the surface oxidises (compare the bottom with the two upper spectra), signifying a transformation from atomic oxygen to lattice oxygen. Assuming  $\alpha$  and  $\beta$  peaks are gas phase formaldehyde, their shifts in apparent binding energy correspond to an increase in work function as the surface oxidises.<sup>19,33</sup> From the direction of the shift we can conclude that the work function of adsorbate-covered metallic Cu surface is higher than the adsorbate-covered oxidised Cu surface.

Although water is not an oxidiser itself, here it indirectly causes the surface to oxidise when added to the methanol and oxygen gas mixture. At first glance, this might be considered as a site blocking mechanism: OH competes for adsorption sites with methoxy, thereby lowering the amount of reducing methoxy species on the surface. However, this interpretation is not consistent with the

observations of Fig. 5, in which we can observe considerable amounts of methoxy on the surface. We rather attribute the surface

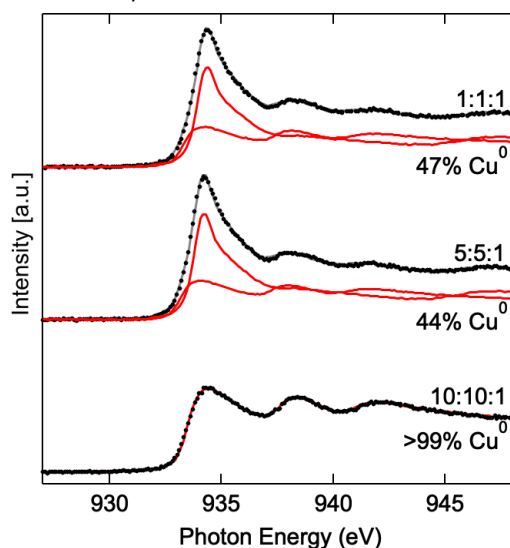


**Fig. 6** Cu  $L_3$  edge of the x-ray absorption spectra at 200 °C sample temperature in the presence of 0.15 mbar methanol vapour, 0.15 mbar water vapour, and 0.015 mbar, 0.03 mbar, or 0.15 mbar oxygen (presented as partial pressure ratios). The surface starts to oxidise at higher oxygen partial pressures. The red curves show the relative contributions of the  $\text{Cu}^0$  and  $\text{Cu}_2\text{O}$  reference spectra to the linear combination fit. The significant differences in the chemical state observed between Fig. 4 and Fig. 6 at same oxygen partial pressures are due to the presence of water vapour.

oxidation to a shift of equilibrium in one of the critical reaction steps:  $\text{CH}_3\text{OH}(\text{ad}) + \text{O}(\text{ad}) \leftrightarrow \text{OCH}_3(\text{ad}) + \text{OH}(\text{ad})$ . As more OH is adsorbed on the surface, there will be shift towards the left hand side, hence more atomic oxygen is left available on the surface for  $\text{Cu}_2\text{O}$  formation. In other words, during the transient state, the rate of the  $2\text{Cu} + \text{O}(\text{ad}) \rightarrow \text{Cu}_2\text{O}$  reaction is comparable with the  $\text{CH}_3\text{OH}(\text{ad}) + \text{O}(\text{ad}) \rightarrow \text{OCH}_3(\text{ad}) + \text{OH}(\text{ad})$  reaction rate, when there is excess OH on the surface due to gas phase water that is present. According to this assumption, one might also then expect less methoxy and formate on the surface. However, we note that the XPS spectra of Fig. 5 were acquired in near steady-state conditions when the surface was already oxidised, so the methoxy and formate intensities in Fig. 5 primarily depend on their adsorption energy on  $\text{Cu}_2\text{O}$ .

## 4. Conclusions

In this work, we studied the chemical state and the nature of the adsorbed species on polycrystalline Cu foils at 200 °C in the presence of methanol, water, and oxygen under conditions representative of methanol conversion reactions. We find that:

- 1- At 200 °C, no methanol derivatives adsorb on the Cu surface when only methanol vapour is present in the gas phase. The surface has to be cooled down, e.g. to 65 °C to start observing methoxy and formate adsorption.
- 2- Methoxy and formate cover the surface when oxygen gas is present with methanol vapour at 200 °C sample temperature, with more formate observed at higher oxygen partial pressures.
- 3- The surface remains largely metallic under the methanol oxidation conditions used in this study (sample temperature = 200 °C, 0.15 mbar methanol, 0.015–0.15 mbar  $\text{O}_2$ ). This is in stark contrast with

the chemical state of the surface under CO oxidation reaction conditions,<sup>18</sup> where the surface oxidises to  $\text{Cu}_2\text{O}$  even at lower temperatures and oxygen-lean conditions. We attribute this difference to methanol being a much more effective reducing agent than CO. Moreover, the methoxy and atomic oxygen adsorption energies are comparable on metallic Cu, an ideal situation for a Langmuir-Hinshelwood type reaction mechanism for further oxidation of methoxy.

4- When water vapour is added to the methanol vapour and oxygen mixture (0.15 mbar methanol, 0.15 mbar  $\text{H}_2\text{O}$ , 0.015–0.15 mbar  $\text{O}_2$ ) at 200 °C, the Cu surface oxidises towards to  $\text{Cu}_2\text{O}$  for higher oxygen partial pressures (Cu oxidation is not observed without the addition of water vapour). We attribute this to the shift in equilibrium leading to less atomic oxygen being consumed by reaction with methanol on the surface, meaning more atomic oxygen is instead available to feed oxidation of the Cu catalyst.

Our observations highlight the importance of probing catalyst chemical state and the absorbed species present under realistic reaction conditions, as seemingly modest changes to the reaction environment (water addition in this case) can alter these in unexpected ways. Such effects are not captured by ex situ measurements where the catalyst's surface chemistry can be altered as the reaction environment is removed. The continued development of in situ and operando interface-sensitive spectroscopic techniques thus promises significant improvements in our molecular level understanding of the complex chemistry occurring on surfaces, particularly as these techniques begin to reach the atmospheric pressure regime that is closer to most industrial reactions.<sup>31</sup>

## Conflicts of interest

There are no conflicts to declare.

## Acknowledgements

This work was supported by the Israel Science Foundation's (ISF) Research Grant No. 919/18 and Weizmann - UK Making Connections Programme. BE acknowledges the support from the Zuckerman STEM Leadership Faculty Fellowship, Ruth and Herman Albert Scholarship Program for New Scientists, and the Abramson Family Center for Young Scientists. JSL acknowledges the support from the Weizmann Institute "la Caixa" Foundation postdoctoral fellowship support. RSW acknowledges support from a CAMS-UK fellowship. We acknowledge Diamond Light Source for time on Beamline B07C under proposal SI19299-1.

## References

- 1 G. A. Olah. *Angew. Chem. Int. Ed.*, 2005, **44**, 2636–2639.
- 2 K. L. Hohn and Y. C. Lin. *ChemSusChem*, 2009, **2**, 927–940.
- 3 H.-Y. Tang, P. Erickson, H. C. Yoon and C.-H. Liao. *Int. J. Hydrogen Energy*, 2009, **34**, 7656–7665.
- 4 D. A. Outka, R. J. Madix and J. Stöhr. *Surf. Sci.*, 1985, **164**, 235–259; M. Bowker. *Top. Catal.*, 1996, **3**, 461–468; J. P. Camplin and E. M. A. McCash. *Surf. Sci.* 1996, **360**, 229–241.
- 5 I. E. Wachs and R. J. Madix. *J. Catal.*, 1978, **53**, 208–227; A. F. Carley, A. W. Owens, M. K. Rajumon, M. W. Roberts and S. D.

- Jackson. *Catal. Lett.*, 1996, **37**, 79-87; T. H. Ellis and H. Wang. *Langmuir*, 1994, **10**, 4083-4088.
- 6 V. I. Bukhtiyarov, I. P. Prosvirin, E. P. Tikhomirov, V. V. Kaichev, A. M. Sorokin and V. V. Evstigneev. *Catal. Lett.*, 2003, **79**, 181-188.
  - 7 T. Schedel-Niedrig, T. Neisius, I. Böttger, E. Kitzelmann, G. Weinberg, D. Demuth and R. Schlögl. *Phys. Chem. Chem. Phys.*, 2000, **2**, 2407-2417; A. Knop-Gericke, M. Hävecker, T. Schedel-Niedrig, R. Schlögl. *Top. Catal.*, 2001, **15**, 27-34.
  - 8 H. Bluhm, M. Hävecker, A. Knop-Gericke, D. Teschner, E. Eleimenov, V. I. Bukhtiyarov, D. F. Ogletree, M. Salmeron and R. Schlögl. *J. Phys. Chem. B*, 2004, **108**, 14340-14347.
  - 9 M. Fang, G. Santos, Z. Chen and S. Baldelli. *Surf. Sci.*, 2016, **648**, 35-41.
  - 10 B. Eren, H. Kersell, R. S. Weatherup, C. Heine, E. J. Crumlin, C. Friend and M. Salmeron. *J. Phys. Chem. B*, 2018, **122**, 548-554.
  - 11 I. P. Prosvirin, A. V. Bukhtiyarov, H. Bluhm, V. I. Bukhtiyarov. *Appl. Surf. Sci.*, 2016, **363**, 303-309.
  - 12 H. Chi, C. M. Andolina, J. Li, M. T. Curnan, W. A. Saidi, G. Zhou, J. C. Yang and G. Vesper. *Appl. Catal. A*, 2018, **556**, 64-72.
  - 13 L. Trotochaud, A. R. Head, S. Pletincx, O. Karsligolu, Y. Yu, A. Waldner, L. Kyhl, T. Hauffman, H. Terryn, B. Eichhorn and H. Bluhm. *J. Phys. Chem. B*, 2018, **122**, 1000-1008.
  - 14 P. Jiang, D. Prendergast, F. Borondics, S. Porsgaard, L. Giovanetti, E. Pach, J. Newberg, H. Bluhm, F. Besenbacher, M. Salmeron. *J. Chem. Phys.*, 2013, **138**, 024704.
  - 15 Hävecker, M. Cavalleri, M. Herbert, R. Follath, R. Knop-Gericke, A. Hess, C. Hermann, K. Schlögl, R. *Phys. Status Solidi Basic Res.* **2009**, **246**, 1459-1469.
  - 16 Ashley, J. C. Tungst, C. J. Ritchie, R. H. Anderson, V. E. *IEEE Trans. Nucl. Sci.* **1976**, **NS-23**, 1833-1837; Frazer, B. H. Gilbert, B. Sonderegger, B. R. De Stasio, G. *Surf. Sci.* **2003**, **537**, 161-167.
  - 17 R. D. Leapman, L. A. Grunes and P. L. Fejes. *Phys. Rev. B*, 1982, **26**, 614; M. Grioni, J. F. van Acker, M. T. Czyzyk and J. C. Fuggle. *Phys. Rev. B*, 1992, **45**, 3309.
  - 18 B. Eren, C. Heine, H. Bluhm, G. A. Somorjai and M. Salmeron. *J. Am. Chem. Soc.*, 2015, **137**, 11186-11190.
  - 19 S. Axnanda, M. Scheele, E. Crumlin, B. Mao, R. Chang, S. Rani, M. Faiz, S. Wang, A. P. Alivisatos and Z. Liu. *Nano Lett.*, 2013, **13**, 6176-6182.
  - 20 Z. Besharat, J. Halldin Stenlid, M. Soldemo, K. Marks, A. Önsten, M. Johnson, H. Öström, J. Weissenrieder, T. Brinck and M. Göthelid. *J. Chem. Phys.*, 2017, **146**, 244702.
  - 21 M. Wiklund, A. Jaworowski, F. Strisland, A. Beutler, A. Sandell, R. Nyholm, S. L. Sorensen, J. N. Andersen. *Surf. Sci.* 1998, **418**, 210-218.
  - 22 A. F. Carley, A. W. Owens, M. K. Rajumon, M. W. Roberts and S. D. Jackson. *Catal. Lett.*, 1996, **37**, 79-87.
  - 23 Ch. Ammon, A. Bayer, G. Held, B. Richter, Th. Schmidt and H.-P. Steinrück. *Surf. Sci.* 2002, **507-510**, 845-850.
  - 24 X. Deng, A. Verdaguer, T. Herranz, C. Weis, H. Bluhm and M. Salmeron. *Langmuir*, 2008, **24**, 9474-9478.
  - 25 H.-J. Freund, G. Meijer, M. Scheffler, R. Schlögl and M. Wolf. *Angew. Chem. Int. Ed.*, 2011, **50**, 10064-10094.
  - 26 S. Sakong, Methanol Oxidation on Oxygen Covered Cu Surfaces. Ph.D. Thesis, Technische Universität München, 2005; R. A. Hoyt, M. M. Montemore, E. C. H. Sykes, E. Kaxiras. *J. Phys. Chem. C*, 2018, **122**, 21952-21962.
  - 27 S. Vollmer, G. Witte, Ch. Wöll. *Catal. Lett.*, 2001, **77**, 97-101.
  - 28 B. Eren, L. Lichtenstein, C. H. Wu, H. Bluhm, G. A. Somorjai and M. Salmeron. *J. Phys. Chem. C*, 2015, **119**, 14669-14674; A. Soon, M. Todorova, B. Delley and C. Stampfl. *Phys. Rev. B*, 2006, **73**, 165424; X. Duan, O. Warschkow, A. Soon, B. Delley, C. Stampfl. *Phys. Rev. B*, 2010, **81**, 075430.
  - 29 R. S. Weatherup, C. H. Wu, C. Escudero, V. Pérez-Dieste, M. B. Salmeron, *J. Phys. Chem. B*, 2017, **122**, 737-744.
  - 30 S. Royer and D. Duprez. *ChemCatChem*, 2011, **3**, 24-65.
  - 31 R. S. Weatherup, B. Eren, Y. Hao, H. Bluhm and M. B. Salmeron. *J. Phys. Chem. Lett.*, 2016, **79**, 1622-1627.
  - 32 C. Wu, B. Eren, and M. B. Salmeron. *Topics in Catalysis*, 2016, **59**, 405-419.
  - 33 C. Wu, B. Eren, H. Bluhm and M. B. Salmeron. *ACS Catalysis*, 2017, **7**, 1150-1157.